1 **Configuration of Coupling Methanol Steam Reforming over Cu-Based Catalyst**

2 **in a Synthetic Palladium Membrane for One-Step High Purity Hydrogen**

3 **Production**

4 Chao Wang[1,*], Jiahong Weng[1], Mingzheng Liao[1], Qiang Luo[1], Xianglong Luo[1],

5 Zhipeng Tian[1], Riyang Shu[1], Ying Chen[1], Yanping Du[2,**]

6

7 1. Guangdong Provincial Key Laboratory on Functional Soft Condensed Matter,

8   School of Materials and Energy, Guangdong University of Technology,

9   Guangzhou 510006, China

10 2. China-UK Low Carbon College, Shanghai Jiao Tong University, Shanghai

11   200240, China

12 **Abstract**

13 Methanol steam reforming coupled with an efficient hydrogen purification

14 technology to produce high purity hydrogen that feeds for hydrogen fuel cells is an

15 attractive approach to realizing distributed power generation. However, the harmony of

16 catalytic reforming and hydrogen separation with respect to thermodynamics is still an

17 issue. In this work, in order to construct an integrated methanol steam reforming (MSR)

18 reactor for high purity hydrogen production, $CuCe/Al_2O_3$ was synthesized by a

19 hydrothermal-impregnated method and a Pd membrane supported by a porous ceramic

20 using the electroless plating method. The results revealed that the catalytic activity and

21 high temperature stability for methanol steam reforming were evidently improved by

22 tuning the copper dispersion, porous structure and the crystal phase. The coupling range

23 with palladium membrane operating temperature was widened. $CuCe/Al_2O_3$ presented

an excellent stability with a better carbon deposition resistance for the long-term tests than Cu/Al_2O_3, which exhibited 836.68 $\mu mol/g_{cat}\cdot min$ of H_2 production with low carbon deposition (3.38 wt.%) and lower CO emission (0.48 vol.%). A 10 μm thick Pd membrane that was deposited on the ceramic support displayed dense and even surface morphology. The effect of palladium membrane structure on hydrogen separation was analyzed. In addition, the influence of temperature on coupling was discussed. Ultimately, high purity of H_2 (99.36 vol.%) was achieved at 400 °C by integrating the Pd membrane reactor with methanol steam reforming. The internal temperature distribution of the reactor and the effects of feeding conditions were also investigated. This work might offer certain reference for the development of the future distributed integrated hydrogen power generation system, especially in the application of electric vehicles and on-site electricity.

Keywords

High purity hydrogen production; Methanol steam reforming; Palladium membrane; $CuCe/Al_2O_3$

1.Introduction

Nowadays, hydrogen plays an irreplaceable role for its efficient and clean properties as an energy carrier [1]. The global demand for hydrogen is gradually increasing and is expected to exceed 500 million metric tons by 2070 [2]. From the perspective of application, hydrogen production from low-carbon alcohols with high hydrogen and low sulfur contents has great potential for development. Compared with

gaseous hydrogen carriers, methanol as an inexpensive hydrocarbon liquid hydrogen carrier (low-carbon alcohols) with a high hydrogen content, is able to react with water and release H_2 under relatively mild conditions owing to its absence of a strong C-C bond compared to other multi-carbon hydrocarbons resources [3]. In addition to the methanol steam reforming reaction (MSR, R1), there are two main side reactions, methanol decomposition (MD, R2) and water gas shift reaction (WGS, R3) which brings undesirable by-products [4]:

$$CH_3OH+H_2O\rightarrow CO_2+3H_2 \qquad \Delta H=49.7kJ/mol \qquad (R1)$$

$$CH_3OH\rightarrow CO+2H_2 \qquad \Delta H =90.2kJ/mol \qquad (R2)$$

$$CO_2+H_2O \leftrightarrow CO_2+H_2 \qquad \Delta H=-41.2kJ/mol \qquad (R3)$$

Except macroscopic reaction conditions such as feeding compositions, the catalytic bed temperature, the space velocity etc., these reaction pathways are mostly determined by the nature of the catalyst (including the sorts of support and active metal components) which further affect the hydrogen production [5]. In fact, due to the restriction of thermodynamic equilibrium, it is not adequate to achieve high purity hydrogen merely relying on the catalysts [6]. The resultant crude hydrogen still needed to be further purified by means of chemical or physical separation for industrial purpose [7]. Therefore, it is essential to implement appropriate catalysts and effective separation methods for the regulation of reaction paths and the separation of impurity gases in the process of obtaining high-purity hydrogen.

Compared to traditional separation processes (such as pressure swing adsorption, secondary selective catalytic conversion), membrane separation technology is suitable for distributed hydrogen energy system owing to it possesses simple operation, compactness and lightweight, continuous flow, favorable thermal compatibility [8]. Pd-based membranes are mostly used for ultra-high H_2 purification due to their high H_2

permeances and selectivities compared to other materials. These membranes may be classified into unsupported and supported ones. Researchers generally prefer to use supported pd membranes for higher mechanical stability and lower cost [9]. Therefore, the selection of the support is of critical importance in the preparation of defect-free pd membranes. Porous ceramic supports, having a gradual reduction in pore size from the bulk to the top layer, have a good surface quality to support very thin Pd-based membranes. It has better mechanical and thermal stability than metallic supports and Vycor glass supports [10].

In traditional reactors, hydrogen production and purification are carried out separately, and syngas is passed into palladium tube to separate impurities. Due to the limitations of thermodynamics, kinetics and heat transfer, it is difficult to achieve high methanol conversion and purification efficiency simultaneously [11]. It is possible to combine reactions and preferential product (hydrogen) separation in a single operation in a Pd-based membrane reactor. The advantages of the Pd-based membrane reactors lie on their capability to extract hydrogen from the product stream and overcome thermodynamic and kinetic limitations in the reaction zone with high efficiency, structural compactness and high heat utilization, etc [12].

However, the compatible of both processes on working temperature is still an issue owing to MSR reaction running at a relative mild condition (200-250 °C) while the purification process with Pd membrane generally operates at 400-500 °C [13]. Pd membrane works at lower 298 °C would easily cause membrane splitting (hydrogen embrittlement) because of the formation of the β-phase hydride, which has a considerably expanded lattice compared with α-phase [14]. In general, there are two approaches to realize the temperature coupling. One is improving the catalytic process by developing a high temperature stable catalyst, the other is lowering the purification

temperature by synthesizing a Pd-Ag alloy membrane to adept the MSR [15]. However, it is worth noting that synthesizing or developing a low temperature Pd based membrane is normally more complicated in the process and costly than the former, while the MSR reaction can be catalyzed by low-cost metal catalysts such as Cu, Zn, Ni, etc. Hence, it is a relatively economical and reliable method to develop a high temperature stable catalyst to adapt the working condition of Pd membrane reactor. It should be noted that thermodynamic conditions, especially temperature is one of the important factors affecting the coupling of catalyst and palladium membrane. Shu et al. [16] found that the hydrogen separation efficiency of palladium membrane had different effects on methane conversion at different temperatures. At a moderate temperature of 500-600 °C, membrane separation can result in a great improvement on the MSR equilibrium. Therefore, it is necessary to develop a suitable catalyst and find the best coupling conditions. In addition, the establishment of appropriate porous structure and mechanical stability of palladium membrane is the key to further improve the gas molecule transfer efficiency [17].

Compared to the other common low-cost metal catalysts, Cu catalysts could exhibit higher selectivity towards MSR reaction (R1) due to adsorbed intermediate HCHO (formaldehyde) species react with water to directly produce H_2 and CO_2 without forming a CO intermediate [18]. It is necessary to regulate the product compositions to improve the separation efficiency of palladium membrane. Cu-based catalyst has strong ability to influence reaction pathways of reforming reaction because of its excellent selectivity. Nevertheless, Cu active species tend to be destructed and agglomerated due to thermal sintering at high temperature [19]. Therefore, it is necessary to improve the high temperature stability of Cu-based catalysts and adjust the catalyst components to better coupling with palladium membrane.

Improving the dispersion of Cu-species by employing Al_2O_3 as a support would be a viable approach to resisting sintering because of its high surface area (>200 m^2/g) and the thermal stability [20]. The gas selectivity of Cu-based catalyst was found to be strongly dependent on the reduction state of the Cu and its dispersion over the support, which further affected the adsorption and the activation of methanol [21]. In alumina supported catalysts, the active catalyst components remain dispersed to a large extent within the pores of the support [22]. The pore size of the alumina support, therefore, plays a crucial role in influencing the activity of the catalyst. In recent years, hydrothermal technology has been considered as an alternative method for the modification of γ-Al_2O_3 support. The hydrothermal pretreatment of the impregnation sample prior to the sintering would be an effective method to produce alumina-supported copper catalysts with superior activities [23]. Stanislaus et al. [22] found that the synthesized NiMo/γ-Al_2O_3 with large pores by hydrothermal modification of γ-Al_2O_3 would avoid the rapid deactivation in the hydrotreating process of the residual oil. Ceria is also a modifier affecting the degree of dispersion as well as the redox behavior and catalytic activity of supported catalysts [24]. CeO_2 has been found viable to increase the thermal stability and the activity of Al_2O_3-supported Cu catalysts through a synergetic effect and to favor the conversion of CO via the WGS reaction (R3) [25].

The present study focused on improving the high temperature activity and stability of Cu/Al_2O_3 catalysts and regulating the composition of gas products to further enhance the coupling with palladium membrane purification. Moreover, the thermal coupling conditions between catalyst and palladium membrane reactor were studied. The prepared catalysts were experimentally examined under various reaction conditions in a fixed-bed reactor while the characterization of the catalysts and the palladium

membrane for detailed morphologies and microstructures were carried out by XRD, BET, FESEM, etc. The carbon deposition over the spent catalysts was tested by the TGA analysis. Based on these studies, we have proposed an explanation for the MSR behavior exhibited by these catalysts by correlating their activity pattern with the microstructural features and the surface information obtained from characterization analysis. Furthermore, the catalyst and palladium membrane were integrated into a hydrogen-purification integrated reactor to achieve a greatly efficient hydrogen production and purification. The thermal coupling effect between the catalyst and the palladium membrane was investigated in this research. The reactor was tested for purification at different temperatures, and the stability test was carried out at 400 °C. The internal temperature distribution of the reactor and the effects of feeding conditions were also studied.

2.Experimental

2.1. Chemicals and materials

In this work, all chemicals were of analytical grade and used as received without further purification. Spherical γ-Al$_2$O$_3$ (5 mm diameter) was purchased from Tianjin Kemiou Chemical Reagent Co., Ltd. Cerium nitrate hexahydrate (Ce(NO$_3$)$_3$·6H$_2$O), copper nitrate trihydrate (Cu(NO$_3$)$_2$·3H$_2$O) were purchased from Shanghai Macklin Biochemical Co., Ltd. Porous ceramic tubes (12 mm OD, 8 mm ID, 0.2 μm pores) were used as the support of Pd membrane, which were purchased from Hefei Yijiete Membrane Technology Co., Ltd. The chemicals used in the plating solutions were PdCl$_2$, NH$_4$OH, NH$_4$Cl, and NaH$_2$PO$_2$ purchased from Tianjin Zhiyuan Chemical Reagent Co., Ltd.

2.2. Synthesis of catalysts

The γ-Al$_2$O$_3$ support was modified according to the literature procedure [26] and

catalysts were synthesized according to our previous report [27]. Firstly, spherical γ-Al_2O_3 were added to a specific concentration of PEG-4000 solution, then the sample was stirred for 30 minutes under 60 °C. Afterwards, the mixture was transferred to a polytetrafluoroethylene container sealed with a high-pressure reactor and placed in a drying oven at 100 °C for 5 hours. The obtained sample was filtered and dried at 90 °C for 6 hours. For the last step, the sample was calcined at 400 °C for 4h in muffle furnace to obtain the modified γ-Al_2O_3 support, hereafter named Al_2O_3-H. Next, unmodified and modified support were impregnated in a solution containing a certain amount of $Ce(NO_3)_3 \cdot 6H_2O$ and $Cu(NO_3)_2 \cdot 3H_2O$. The solution was then heated to 60 °C and agitated for 30 minutes. The impregnated precursor was filtered out and dried at 80 °C for 12 hours before being calcined at 400 °C for 4 hours in a muffle furnace to obtain two composite catalysts. The obtained catalysts were denoted as $CuCe/Al_2O_3$ and $CuCe/Al_2O_3$-H, respectively.

A Cu/Al_2O_3 catalyst was synthesized using the impregnation procedure as a comparison. Following the identical method as previously, The γ-Al_2O_3 support without hydrothermal modification was impregnated in a $Cu(NO_3)_2 \cdot 3H_2O$ aqueous solution.

2.3. Preparation of supported Pd-membrane

The supported palladium membrane was prepared by the electroless plating technique. To clean the porous ceramics tubes of dirt and contaminants adsorbed within the pores, the following cleaning procedure was used. The porous ceramics tubes were cleaned using an ultrasonic bath with acidic solution and alkaline solution successively, followed by rinsing in deionized water, then the supports were dried overnight at 120°C. Finally, they were roasted at 550 °C for 6 h in a muffle furnace.

The porous ceramics tubes were activated prior to electroless plating. The activation process involved immersion of the supports in a dilute 5 mM Sn(II) solution

for 5 min, followed by 5 min rinsing in flowing deionized water. The supports were then immersed in 5 mM Pd(II) solution for 5 min, followed by another 5 min rinsing in flowing deionized water. The first step sensitized the support, while the second step activated it by nucleating Pd seeds onto its surface. The pH of the sensitizing and seeding solutions were kept between 4 and 5 by addition of hydrochloric acid. To achieve an activated support that was uniformly distributed, the process was repeated multiple times.

Followed the activation step, palladium was simultaneously deposited on the substrate by electroless plating. The plating bath consisted of palladium chloride, ammonium chloride as a chelating agent and sodium hypophosphite as the reducing agent. The pH value of the electroless plating solution was adjusted by ammonia. The solution in the plating bath was stirred with a magnetic stirrer and the plating temperature was controlled in an oven at 50 °C. After the reaction was completed, the supported palladium membranes were removed and rinsed with deionized water, then soaked in ethanol solution for a period, and then washed with deionized water. Finally, they were dried in an oven at 120 °C for 12 h.

2.4. Characterization

The gaseous products were collected by sample bags with 500 ml of volume size and then, analyzed offline by a gas chromatograph (GC-2014c, Shimadzu, Japan). The surface morphologies of the sample were characterized by SU 8100 scanning electron microscopy (SEM). The surface areas and pore size distribution of the catalysts were determined by nitrogen adsorption using an ASAP 2020 system (Micromeritics Instruments Corporation). The surface area was calculated using the BET method while the pore size distribution was obtained from the adsorption isotherm by the BJH method. Powder X-ray diffraction (XRD) patterns were obtained by D8 Advance diffractometer

1 equipped with a Cu-Kα radiation, at a scanning rate of $10°$ min^{-1}. The scanning angle

2 ranges from 10 to 80 degrees.

3 *2.5. Catalytic activity test*

4 Hydrogen production from methanol steam reforming was conducted in a fixed-

5 bed experimental setup indicated in Fig. 1 (a). A particular flow of methanol aqueous

6 solution was supplied once the furnace temperature was reached to the reaction

7 temperature. The methanol aqueous solution with a water to alcohol ratio of 1.2:1 (mole

8 ratio) was heated by steam at 200 °C, and then pumped into the tube furnace with

9 nitrogen gas at a flow rate of 100 ml/min, nitrogen gas flow was monitored by a mass

10 flowmeter. The tube furnace and liquid deliver system were connected by the steel tube,

11 and the steel tube was insulated by the heating belt. 10 g of fresh catalyst was placed

12 into reaction tube (length: 30 cm, inner diameter: 17 mm) for SMR reaction at

13 atmospheric pressure and the temperature was controlled by a K-type thermocouple.

14 Prior to each run, the catalyst was reduced at 250 °C with a mixture of 20vol.% H_2/N_2

15 at a flow rate of 300 ml/min for 1 hour. Another K-type thermocouple was placed in the

16 reaction tube so as to monitor the catalyst bed temperature. The condenser and filter

17 units were set for the removal of steam and other liquid impurities during reaction. The

18 gaseous products were collected at various points in time by sample bags with 500 ml

19 of volume size and then, analyzed offline by a gas chromatograph (GC-2014c AT,

20 Shimadzu, Japan) equipped with a TDX-01 and Poraplot Q column that were connected

21 in series with a thermal conductivity (TCD) and flame ionization detector (FID),

22 respectively.

23 *2.6. Steam reforming in hydrogen-purification integrated reactor*

24 Fig. 1(b) and 1(c) displayed the schematic diagram and photograph of the

25 hydrogen-purification integrated reactor used in this study, respectively. One end of the

1   membrane tube was connected to a stainless steel tube, and then loaded into a quartz

2   tube. The stainless steel tube was connected to the quartz tube with a heat-resistant and

3   pressure-resistant silica gel plug. 10g catalysts were placed into the quartz tube and then

4   reduced under the same conditions of the catalyst test. The reactor was placed in a tube

5   furnace as shown in Fig. 1 for methanol steam reforming. Before reaction, the reactor

6   was slowly heated to 673 K at a rate of 1 K min^{-1}, afterwards methanol and water vapor

7   was gradually introduced to the reactor. The test was conducted in the temperature range

8   of 360-440°C and a trans-membrane pressure difference of 300 kPa. The flux on the

9   permeate side was measured with bubble film gas meters and theoretically calculated

10 according to product selectivity. The concentration of products on the permeate side

11 was monitored offline by gas chromatograph (GC-2014c AT, Shimadzu, Japan).

12 **3. Results and discussion**

13 *3.1. Pore structure and BET surface areas*

14   N_2 physical adsorption-desorption isotherms of fresh catalysts were shown in Fig.

15 2(a). All samples were classified as type IV isotherms according to IUPAC

16 classification, indicating the presence of mesoporous structures. The synthetic catalysts

17 all belong to H2 hysteretic rings, showing that their pore sizes were wide and in various

18 pore type distributions, such as "ink bottle" pore, tubular pore with uneven pore sizes

19 and densely packed spherical particle gap pore [28]. Table 1 summarized the pore

20 structure parameters of synthetic catalysts. As it is clear, CuCe/Al_2O_3-H had the largest

21 specific surface area (254.36 m^2g^{-1}) and pore size (6.69 nm). It should be noted that

22 larger surface areas can enhance the dispersion of active phases, provide the uniformity

23 of small nanoparticles and lead to superior catalytic performance [29]. After

24 hydrothermal treatment, the BET specific surface area of the sample decreased to a

25 certain extent, but the mean pore diameter and the pore volume increased. It is widely

known that primary crystal formation can result in a reduction in the specific surface

area of Al_2O_3 [30]. As a result, the formation and maturation of boehmite crystals during

the hydrothermal modification should be primarily responsible for the textural

alterations of the support described above. Fig. 2 (b) displayed the pore size distribution

curves of the catalysts. It is apparent that following the hydrothermal treatment, the

pore size distributions begin to expand. $CuCe/Al_2O_3$-H had the widest pore size

distribution (between 2 nm and 16 nm). Broad pore size distributions, such as those

seen in $CuCe/Al_2O_3$-H may offer various transportation channels for distinct reactants

and intermediates while reducing internal diffusion resistance [31].

The influence of palladium deposition on the structural characteristics of porous

ceramic support was also examined. Fig. 3 (a) depicts the N_2 physical adsorption-

desorption isotherms of the supported palladium membrane and the ceramic support.

The resulting isotherm, which belongs to type IV, exhibited features of a mesoporous

membrane going through capillary condensation. A tight pore size distribution is

necessary for excellent selectivity of palladium membrane [32]. The pore size

distribution curves of the supported palladium membrane exhibited a narrow pore size

distribution, as shown in Fig. 3(b). This indicated that the palladium membrane samples

had relatively uniform pore sizes. The pore structure parameters of supported palladium

membranes were presented in Table 1. The effects of the palladium deposition were

shown in the observation that there was an increment in surface area and a decrease in

pore width from 16.94 to 16.72 nm. The separation selectivity of palladium membranes

was further improved by the increased surface area and the decreased pore diameter

[33].

3.2. SEM analysis

The Surface morphology of the samples was presented in Fig. 4 and the elemental

1 composition and content of each catalyst was listed in Table 2. Comparison of Cu/Al_2O_3

2 and $CuCe/Al_2O_3$ revealed that the doping of cerium enhanced the loading of copper on

3 the catalyst surface. As shown, $CuCe/Al_2O_3$-H had a lower copper load of 5.15 wt.%.

4 He et al. [34] found that Cu-based catalyst with a 5% copper load had the best dispersion,

5 and TPR results showed that it had comparatively high catalytic activity due to the fairly

6 low reduction temperature peaks. Comparing the samples with and without

7 hydrothermal treatment, the particle size of the former was prominently smaller than

8 that of the latter, and the agglomeration of the particles was greatly restrained by the

9 hydrothermal modification. From the XRD results, the reason for the above

10 phenomenon was that the increase of crystallinity of the catalyst through hydrothermal

11 modification enhanced the thermal stability and inhibited the sintering of the catalyst

12 [35]. The copper element mapping of the catalysts was analyzed, and the results were

13 shown in Fig. 5. Meanwhile, the grayscales distribution of copper elements was plotted

14 along X-axis and Y-axis, respectively. The grayscales of copper element distribution

15 were processed and calculated by MATLAB. It is clear that the standard deviation of

16 $CuCe/Al_2O_3$ along X-axis and Y-axis was decreased compared to that of Cu/Al_2O_3. It

17 meant that the copper distribution was more uniform due to the addition of cerium.

18 $CuCe/Al_2O_3$-H had the smallest standard deviations along both axes (S=1.76 at X-axis

19 and S=1.43 at Y-axis), meaning that hydrothermal treatment led to a better copper

20 dispersion.

21 Fig. 6 showed micrographs of the top surface and cross section of supported

22 palladium membranes. The palladium particles deposited on the porous support (cf. Fig.

23 6(a)) formed a dense membrane during 2 hours of electroless plating. The palladium

24 particle scale varied over the thickness of the palladium membrane and gradually

25 increased from inside to outside, according to the SEM micrograph of the cross section.

1   The uniform and compact microstructure displayed in Fig. 6(b) was the consequence

2   of the grain size growing over time in conjunction with sintering and mutualization.

3   The distribution of Pd particle size was shown in Fig. 6(d). The particle size was mainly

4   between 0.8 μm and 1.4 μm. The concentrated particle size distribution indicated that

5   the palladium particle size was uniform, and the maximum particle size can reach up to

6   2.2 μm. The element mapping for the cross section of the supported palladium

7   membrane (Fig. 7) revealed palladium deposition on the exterior of the porous support,

8   as well as in the outer-most pores. It was clearly observed that some palladium particles

9   permeated into the pores of the support, indicating that the palladium membrane was

10   closely bound to the support. According to the scale, palladium membrane thickness

11   was approximately 10 μm.

12   *3.3. XRD analysis*

13   The XRD diffraction pattern of the catalysts were shown in Fig. 8(a). Without prior

14   reduction, the Cu species of prepared catalysts were identified as CuO, and the

15   corresponding peaks were located at 38.50°, 68.02° and 72.24° for the crystal planes of

16   (1 1 1), (2 2 0) and (3 1 1), respectively. Evident overlap between the CuO diffraction

17   peaks and other diffraction peaks points to a low concentration and significant

18   dispersion of Cu species on the catalyst surface. Investigations of methanol adsorption

19   and decomposition on Cu111 surfaces showed that methanol ($CH_3O–H$) undergoes

20   dissociative adsorption to form methoxy species (CH_3O) [36]. It was reported that the

21   generation of methoxy species is promoted by the existence of absorbed O. Some

22   researchers [37] suggested that the O could be available from an incomplete reduction

23   of the catalyst, such as the lattice oxygen of ceria, or from moisture that was present in

1   the methanol feed. The Ce species in $CuCe/Al_2O_3$ and $CuCe/Al_2O_3$-H were recognized

2   as CeO_2. After the addition of cerium, the diffraction peaks of copper oxide became

3   wider, indicating that the addition of ceria reduced the crystalline size of Cu and

4   increased the degree of dispersion. The samples after hydrothermal modification for Al

5   species mostly comprises boehmite crystals, proving that γ-Al_2O_3 was converted to

6   boehmite during the hydrothermal process. The pore size increase of $CuCe/Al_2O_3$-H

7   through hydrothermal treatment was presumably caused by the generation and

8   enlargement of boehmite. The conversion of γ-Al_2O_3 to boehmite under hydrothermal

9   conditions essentially involved rehydration of γ-Al_2O_3 by the uptake of 1 mol H_2O per

10   mole of Al_2O_3 [22]. The diffraction peaks of the samples after hydrothermal treatment

11   became sharp, indicating that the crystallinity of the samples increased. Fig. 8(b)

12   showed the XRD patterns of porous ceramics support and supported palladium

13   membranes. The porous support showed significant diffraction peaks that may be

14   attributed to Al_2O_3 crystals. The sharp peaks of Al_2O_3 indicated the presence of high

15   crystalline phases. It can be seen that the peaks of Al_2O_3 crystals on the supported

16   palladium membrane was dramatically decreased, and an obvious palladium peak can

17   be observed at $40.25°$. These results demonstrated that the porous support had

18   effectively deposited a palladium membrane. The broad diffraction peaks for palladium

19   suggest a tiny size of the crystallites. Metallic palladium was allocated three diffraction

20   peaks. The average size of palladium crystallites calculated from Scherrer's equation is

21   roughly 3 nm, which was smaller than the average pore size of the support.

3.4. Performance test of methanol steam reforming for hydrogen production

In general, the catalytic activity of the catalyst is significantly affected by the MSR temperature [38]. In order to research the influence of temperature on the H_2 generation, the catalytic activity of Cu/Al_2O_3, $CuCe/Al_2O_3$ and $CuCe/Al_2O_3$-H was tested at temperatures between 220 and 400 °C. As displayed in Fig. 9(a), the hydrogen yield of the three catalysts showed a trend of first increasing and then reducing with the increase in temperature. Cu/Al_2O_3 has a larger fluctuation with the change of temperature. This may be due to the sintering of the active components of Cu/Al_2O_3 at high temperature, which caused the reducing of hydrogen yield. It can be seen that $CuCe/Al_2O_3$ had a higher catalytic activity than Cu/Al_2O_3 because the dispersion of Cu was improved by adding cerium. Fig. 9(b) also showed that the gaseous product of $CuCe/Al_2O_3$ had a reduced CO concentration (0.72 vol.% to 0.48 vol.%) because cerium may suppress the methanol decomposition and reverse water gas shift reactions eventually end-up with the low CO and hydrogen rich product stream [39]. The highest H_2 production of three catalysts appeared at 340 °C, 360 °C and 380 °C, respectively. The highest hydrogen production of $CuCe/Al_2O_3$-H reached 836.68 $\mu mol \cdot g_{cat}^{-1} min^{-1}$, which indicated that $CuCe/Al_2O_3$-H had a higher activity at high temperatures.

The catalysts were tested for hydrogen production stability by methanol steam reforming at 400 °C, and the results were shown in Fig. 10. $CuCe/Al_2O_3$ showed high catalytic activity during the early stages of the test before it quickly declined. The high concentration of Cu components (cf. Table 2) may have contributed to the initial high H_2 yield, but with more active components, sintering and carbon deposition proceeded

1 more quickly and intensely, which resulted in a considerable decline in the H_2 yield [25].

2 CuCe/Al_2O_3-H performed more steadily compared to that of Cu/Al_2O_3 and CuCe/Al_2O_3,

3 which exhibited 720.8 $\mu mol \cdot g_{cat}^{-1} min^{-1}$ hydrogen production by the end of 720 min.

4 Compared to that of with Ce-promoter addition, Cu/Al_2O_3 showed a worse stability on

5 hydrogen production, it was kept declining from 895.14 $\mu mol \cdot g_{cat}^{-1} min^{-1}$ to 529.23

6 $\mu mol \cdot g_{cat}^{-1} min^{-1}$ until 720 min while CuCe/Al_2O_3 presented a better performance at the

7 first 60 min, but it finally decreased to 579.02 $\mu mol \cdot g_{cat}^{-1} min^{-1}$. From the results, it can

8 be seen that there was a distinct decrease at the range of 300 to 450 min for Cu/Al_2O_3

9 and CuCe/Al_2O_3, while the CuCe/Al_2O_3-H maintaining stability. Combined with TGA,

10 the decrease in catalyst performance may be mostly owing to sintering caused by

11 prolonged reaction at high temperatures rather than the consequence of carbon

12 deposition (Fig. 11). It demonstrated that the hydrothermal treatment improved the

13 thermal stability of the catalyst. Combined with the analysis of catalyst textural

14 properties in the above section, CuCe/Al_2O_3-H formed a different porous structure and

15 induced a higher specific surface area compared with the remaining two, which might

16 be more beneficial to the diffusion of the reactants, resulting in a more stable hydrogen

17 production. Zeng et al. [40] examined the Cu/ZnO/ZrO_2/Al_2O_3 catalyst in cube-post

18 micro reactors. The results indicate that the highest methanol conversion of 70.27%

19 was achieved at 280 °C. The H_2 concentration in the reformate were around 74.4%, and

20 the CO concentration was about 1%. Shokrani et al. [41] tested the methanol steam

21 reforming performance of a series of CuO/ZnO/Al_2O_3 catalysts, and the catalytic

22 activity decreased from 90% to 60% after 90 hours of reaction at 240 °C. As reported,

23 as long as the catalyst was maintained on reaction for around 12 hours, it could be

24 considered that the catalyst was active and stable [42]. Therefore, the obtained results

25 in this work were competitive and could match the application requirements of electric

1   vehicles and on-site electricity.

2   *3.5. Carbon deposition analysis of spent catalysts*

3   The morphologies of the carbon deposition over the surface of spent catalysts were

4   investigated by FESEM. The images of (d), (f) and (h) in Fig. 4 presented the FESEM

5   images of spent Cu/Al_2O_3, $CuCe/Al_2O_3$ and $CuCe/Al_2O_3$-H samples, respectively. As

6   can be seen, apparent massive agglomeration and sintering appeared in Cu/Al_2O_3. This

7   could be explained by the fact that high temperature led to the sintering of copper

8   crystallites, causing coarsening [43]. The SEM images of the spent $CuCe/Al_2O_3$ catalyst

9   which had been previously exposed to a temperature of 400 °C during the reaction, as

10   depicted in Fig. 4 (f), showed a larger agglomerate of particles in the middle of the

11   image. The distribution of particles showed uniformity over the support. This indicated

12   that the addition of cerium inhibited the sintering of the catalyst. The SEM image of the

13   spent $CuCe/Al_2O_3$-H reacted at 400 °C was reported in Fig. 4(h). It is observed that a

14   uniform distribution of species occurs with smaller agglomerates compared to the spent

15   Cu/Al_2O_3 and $CuCe/Al_2O_3$ catalysts reacted at 400 °C.

16   To learn more about the carbon deposition of the spent catalysts, the thermal

17   gravimetric analysis was conducted in an atmosphere of air. The pyrolysis of the carbon

18   was responsible for the weight reductions in all samples. The weight losses for all

19   samples were attributed to the removal of the deposited carbon. The initial weight loss

20   that occurred before 200 °C was really brought on by the thermolysis of H_2O and CO_2,

21   in addition to the elimination of carbonaceous species such as amorphous carbon, which

22   were quickly oxidized [25]. As shown in Fig. 11, Cu/Al_2O_3 deposited the most weight

23   of carbon (4.14 wt.%), while $CuCe/Al_2O_3$-H has the least carbon deposits (3.38 wt.%).

24   This may be the reason for the best performance of $CuCe/Al_2O_3$-H in long-term reaction

25   at high temperatures. All samples showed a weight loss peak in the DTG profiles about

1 500 °C, which was attributed to the quick decomposition of carbon deposition. These

2 temperatures of weight loss peaks were 496.1 °C, 516.8 °C and 523.4 °C, respectively.

3 Koike et al. [44] suggested that the amorphous carbon could be decomposed at a lower

4 temperature while graphitic carbon was contrary. These peaks should be attributed to

5 amorphous carbon species on the spent catalysts surface. It's obviously shown that the

6 DTG peak position of the Cu/Al_2O_3 and $CuCe/Al_2O_3$ is delayed to a higher temperature

7 in comparison with $CuCe/Al_2O_3$-H. This also meant that the carbon deposited on the

8 Cu/Al_2O_3 and $CuCe/Al_2O_3$ would be more difficult to be gasified than $CuCe/Al_2O_3$-H.

9 *3.6. Performance of catalyst and pd-membrane integrated reactor*

10 Due to the restriction of operating temperature of Pd membrane, the reaction of

11 methanol steam reforming was performed above 360 °C in this study. The product gas

12 permeation concentration per unit area was calculated. The influence of reaction

13 temperature on gaseous product distribution of the hydrogen-purification integrated

14 reactor was shown in Fig. 12(a). Within 360-400 °C, an increase in the reaction

15 temperature monotonically increased the hydrogen concentration. This is ascribed to

16 the fact that a higher temperature favors MSR reaction kinetics as well as H_2 permeation,

17 resulting in a higher separation efficiency. At 400 °C, the hydrogen concentration

18 increased the highest, reaching 99.36 vol.%, and then showed a slight decrease within

19 400-440 °C. The lowest carbon monoxide concentration was 0.07 vol.% at 400 °C, and

20 then increased as the temperature increased. This is because the increase in temperature

21 intensified the MD reaction, thereby increasing the CO concentration on the retentate

22 side. Fig. 12(b) showed the influence of time on stream performance of the hydrogen-

23 purification integrated reactor at 400 °C. Palladium/porous stainless steel membranes

24 generally only operate at around 350 °C, because when the temperature exceeds 400 °C,

25 the intermetallic diffusion occurs between the palladium membrane and the stainless

1 steel support, causing the drop of hydrogen permeance [45]. As shown, compared with

2 the palladium/porous stainless steel membrane, the hydrogen-purification integrated

3 reactor had an excellent stability within 720 min at 400 °C. The hydrogen concentration

4 remained above 99 vol.% for 720 min, which indicated an improved stability and

5 thermal coupling effect with the catalysts of the reactor at high temperatures.

6   To further investigate the reason for the optimal coupling between catalyst and Pd

7 membrane at 400 °C, the internal temperature distribution of the reactor was detected

8 and the results were illustrated in Fig. 13. The lower feed temperature of methanol water

9 vapor results in a progressive rise in the temperature distribution from the entrance to

10 the output. Due to the endothermic characteristics of the methanol steam reforming

11 reaction, the temperature of the catalyst section was between 365 and 385 °C, which

12 was the optimal reaction range for the catalyst. The temperature of the Pd membrane

13 section was above 385 °C, with a temperature difference of about 10 °C. Higher

14 temperature sections and smaller temperature differences were more conducive to

15 stable and efficient hydrogen permeation.

16   The effect of feeding conditions on the purification efficiency of the reactor was

17 also studied. The influences of feeding flux (0.25–3 mL/min) and S/C mole ratio (1.0–

18 1.5) were studied at 400 °C, and the results were shown in the Fig. 14. The methanol

19 conversion can be improved if the S/C mole ratio was raised. Nevertheless, this actually

20 decreased the Hydrogen production of the reactor. The difference was due to the fact

21 that whereas one mole of CH_3OH offer two moles of H_2, one mole of H_2O can only

22 make one mole of H_2. In terms of feeding flux, since methanol conversions were

23 minimal at high feeding flux, the CH_3OH and H_2O species that have been adsorbed on

24 the membrane surface would obstruct the hydrogen separation. As conversion increases

25 (with decreasing space velocity), it means an increase in the catalyst loading or a

1   decrease in the feed flow. The former will lead to an increase in mass and heat transfer

2   resistance, while the latter will increase the partial pressures of CO and CO_2, both of

3   which will hinder Pd membrane purification. Thus, there was the best purification effect

4   at intermediate S/C (1.2) and feeding flux (0.5 mL/min), respectively.

5   **4. Conclusions**

6   In summary, this study investigated the feasibility of methanol steam reforming by

7   coupling $CuCe/Al_2O_3$ with the ceramic supported Pd membrane for integrated one-step

8   high purity hydrogen production. The results displayed that the catalyst support treated

9   by hydrothermal method was beneficial to increasing catalyst surface area and

10 improving copper dispersion. $CuCe/Al_2O_3$ displayed an excellent catalytic performance

11 towards hydrogen production (836.68 $\mu mol \cdot g_{cat}^{-1} min^{-1}$), CO reducing (0.72 vol.% to

12 0.48 vol.%) and slight amount of carbon deposition (3.38 wt.%) under a favorable

13 temperature elevated around 400 °C which is more conducive for coupling with Pd

14 membrane hydrogen separation. High-purity hydrogen production was further obtained

15 with the synthetic 10 μm thickness Pd membrane reactor with increased surface area of

16 the Pd membrane pores. The optimal purification performance was observed at 400 °C

17 with the maximum hydrogen purity of 99.36 vol.%. The internal temperature

18 distribution of the reactor showed that the catalyst and Pd membrane just benefit from

19 their respective most suitable temperature range at the experimental temperature of

20 400 °C. Feeding conditions have a significant impact on reforming reaction and

21 hydrogen permeation. The reactor exhibited the best purification effect at an

22 intermediate S/C mole ratio (1.2) and feeding flux (0.5 mL/min), respectively. This

23 research might shed some light on the development of on board high-purity hydrogen

24 production from methanol steam reforming for the distributed hydrogen fuel cell

25 technology. Future study should pay more attention to the evaluation of technology

1   readiness level considering energy efficiency, cost-benefit, stability of operation.

2

3   **Acknowledgements**

9

1 **References**

2 [1]. Chang Y, Li G, Ma S, et al. Effect of hierarchical pore structure of oxygen carrier

3 on the performance of biomass chemical looping hydrogen generation[J]. Energy,

4 2022: 124301.

5 [2]. Nnabuife S G, Ugbeh-Johnson J, Okeke N E, et al. Present and projected

6 developments in hydrogen production: a technological review[J]. Carbon Capture

7 Science & Technology, 2022: 100042.

8 [3]. Wang G, Wang F, Li L, et al. Experiment of catalyst activity distribution effect on

9 methanol steam reforming performance in the packed bed plate-type reactor[J].

10 Energy, 2013, 51: 267-272.

11 [4]. Zhang H, Xu C, Yu H, et al. Enhancement of methanol steam reforming in a tubular

12 fixed-bed reactor with simultaneous heating inside and outside[J]. Energy, 2022:

13 124330.

14 [5]. Wang C, Chen Y, Cheng Z, et al. Sorption-enhanced steam reforming of glycerol

15 for hydrogen production over a $NiO/NiAl_2O_4$ catalyst and Li_2ZrO_3-based

16 sorbent[J]. Energy & Fuels, 2015, 29(11): 7408-7418.

17 [6]. Mosayebi A, Ahmadi M H E. Combined steam and dry reforming of methanol

18 process to syngas formation: Kinetic modeling and thermodynamic equilibrium

19 analysis[J]. Energy, 2022, 261: 125254.

20 [7]. Fraile D, Lanoix J C, Maio P, et al. Overview of the market segmentation for

21 hydrogen across potential customer groups, based on key application areas[J].

CertifHy Proj, 2015: 1-32.

[8]. Gb A, Ta A, Tdsl A, et al. Recent advances in membrane technologies for hydrogen purification - ScienceDirect[J]. International Journal of Hydrogen Energy, 2020, 45(12):7313-7338.

[9]. Helmi A, Gallucci F, Martin V S A. Resource scarcity in palladium membrane applications for carbon capture in integrated gasification combined cycle units[J]. International Journal of Hydrogen Energy, 2014, 39(20):10498–10506.

[10]. Pal N, Agarwal M, Maheshwari K, et al. A review on types, fabrication and support material of hydrogen separation membrane[J]. Materials Today: Proceedings, 2020, 28: 1386-1391.

[11]. Wang H, Liu M, Kong H, et al. Thermodynamic analysis on mid/low temperature solar methane steam reforming with hydrogen permeation membrane reactors[J]. Applied Thermal Engineering, 2019, 152: 925-936.

[12]. Ji G, Zhao M, Wang G. Computational fluid dynamic simulation of a sorption-enhanced palladium membrane reactor for enhancing hydrogen production from methane steam reforming[J]. Energy, 2018, 147: 884-895.

[13]. Bernardo G, Araújo T, da Silva Lopes T, et al. Recent advances in membrane technologies for hydrogen purification[J]. International Journal of Hydrogen Energy, 2020, 45(12): 7313-7338.

[14]. Yan S, Maeda H, Kusakabe K, et al. Thin palladium membrane formed in support pores by metal-organic chemical vapor deposition method and application to

hydrogen separation[J]. Industrial & engineering chemistry research, 1994, 33(3): 616-622.

[15]. Israni S H, Harold M P. Methanol steam reforming in single-fiber packed bed Pd–Ag membrane reactor: Experiments and modeling[J]. Journal of Membrane Science, 2011, 369(1-2): 375-387.

[16]. Shu J, Grandjean B P A, Kaliaguine S. Asymmetric Pd-Ag/stainless steel catalytic membranes for methane steam reforming[J]. Catalysis Today, 1995, 25(3-4): 327-332.

[17]. Spallina V, Matturro G, Ruocco C, et al. Direct route from ethanol to pure hydrogen through autothermal reforming in a membrane reactor: Experimental demonstration, reactor modelling and design[J]. Energy, 2018, 143: 666-681.

[18]. Yong S T, Ooi C W, Chai S P, et al. Review of methanol reforming-Cu-based catalysts, surface reaction mechanisms, and reaction schemes[J]. International Journal of hydrogen energy, 2013, 38(22): 9541-9552.

[19]. Fornari A C, Menechini Neto R, Lenzi G G, et al. Utilization of sol-gel CuO-ZnO-Al_2O_3 catalysts in the methanol steam reforming for hydrogen production[J]. The Canadian Journal of Chemical Engineering, 2017, 95(12): 2258-2271.

[20]. Papavasiliou J, Avgouropoulos G, Ioannides T. Steady-state isotopic transient kinetic analysis of steam reforming of methanol over Cu-based catalysts[J]. Applied Catalysis B Environmental, 2009, 88(3-4):490-496.

[21]. Garcia G, Arriola E, Chen W H, et al. A comprehensive review of hydrogen

production from methanol thermochemical conversion for sustainability[J]. Energy, 2021, 217: 119384.

[22]. Stanislaus A, Al-Dolama K, Absi-Halabi M. Preparation of a large pore alumina-based HDM catalyst by hydrothermal treatment and studies on pore enlargement mechanism[J]. Journal of Molecular Catalysis A: Chemical, 2002, 181(1-2): 33-39.

[23]. Zhou X, Wang P, Shen Z, et al. Low-temperature NOx reduction over hydrothermally stable SCR catalysts by engineering low-coordinated Mn active sites[J]. Chemical Engineering Journal, 2022, 442: 136182.

[24]. YANG S, HE J, ZHANG N, et al. Effect of rare-earth element modification on the performance of Cu/ZnAl catalysts derived from hydrotalcite precursor in methanol steam reforming[J]. Journal of Fuel Chemistry and Technology, 2018, 46(2): 179-188.

[25]. Wan Y, Zhou Z, Cheng Z. Hydrogen production from steam reforming of methanol over $CuO/ZnO/Al_2O_3$ catalysts: Catalytic performance and kinetic modeling[J]. Chinese Journal of Chemical Engineering, 2016, 24(9): 1186-1194.

[26]. Li J, Lan X, F Xu, et al. Influence of hydrothermally modified γ-Al_2O_3 on the properties of NiMo/γ-Al_2O_3 catalyst[J]. Applied Surface Science, 2008, 254(7):2077-2080.

[27]. Liao M, Chen Y, Cheng Z, et al. Hydrogen production from partial oxidation of propane: Effect of SiC addition on Ni/Al_2O_3 catalyst[J]. Applied Energy, 2019, 252: 113435.

[28]. He Y, Li Z, Xi H, et al. Research progress of gas-solid adsorption isotherms[J]. Ion Exchange and Adsorption, 2004, 20: 376-384.

[29]. Taghizadeh M, Akhoundzadeh H, Rezayan A, et al. Excellent catalytic performance of 3D-mesoporous KIT-6 supported Cu and Ce nanoparticles in methanol steam reforming[J]. International Journal of Hydrogen Energy, 2018, 43(24): 10926-10937.

[30]. Absi-Halabi M, Stanislaus A, Al-Zaid H. Effect of acidic and basic vapors on pore size distribution of alumina under hydrothermal conditions[J]. Applied Catalysis A: General, 1993, 101(1): 117-128.

[31]. Wang C, Jiang Z, Song Q, et al. Investigation on hydrogen-rich syngas production from catalytic co-pyrolysis of polyvinyl chloride (PVC) and waste paper blends[J]. Energy, 2021, 232: 121005.

[32]. Lee B, Komarneni S. Chemical processing of ceramics[M]. CRC press, 2005.

[33]. Orakwe I, Shehu H, Gobina E. Preparation and characterization of palladium ceramic alumina membrane for hydrogen permeation[J]. International Journal of Hydrogen Energy, 2019, 44(20):9914-9921.

[34]. He J, Yang Z, Zhang L, et al. Cu supported on ZnAl-LDHs precursor prepared by in-situ synthesis method on γ-Al_2O_3 as catalytic material with high catalytic activity for methanol steam reforming[J]. International journal of hydrogen energy, 2017, 42(15): 9930-9937.

[35]. Xu H, Liu S, Wang Y, et al. Promotional effect of Al_2O_3 on WO_3/CeO_2-ZrO_2

monolithic catalyst for selective catalytic reduction of nitrogen oxides with ammonia after hydrothermal aging treatment[J]. Applied Surface Science, 2018, 427:656-669.

[36]. Russell Jr J N, Gates S M, Yates Jr J T. Reaction of methanol with Cu (111) and Cu (111) + O (ads)[J]. Surface science, 1985, 163(2-3): 516-540.

[37]. Lin S D, Cheng H, Hsiao T C. In situ DRIFTS study on the methanol oxidation by lattice oxygen over Cu/ZnO catalyst[J]. Journal of Molecular Catalysis A: Chemical, 2011, 342: 35-40.

[38]. Gil M V, Fermoso J, Pevida C, et al. Production of fuel-cell grade H_2 by sorption enhanced steam reforming of acetic acid as a model compound of biomass-derived bio-oil[J]. Applied Catalysis B: Environmental, 2016, 184: 64-76.

[39]. Zhang X, Zhang Y, Wen A, et al. Assessment of soil losses on cultivated land by using the 137Cs technique in the Upper Yangtze River Basin of China[J]. Soil & Tillage Research, 2003, 69(1-2):99-106.

[40]. Zeng D, Pan M, Wang L, et al. Fabrication and characteristics of cube-post microreactors for methanol steam reforming[J]. Applied Energy, 2012, 91(1): 208-213.

[41]. Shokrani R, Haghighi M, Jodeiri N, et al. Fuel cell grade hydrogen production via methanol steam reforming over $CuO/ZnO/Al_2O_3$ nanocatalyst with various oxide ratios synthesized via urea-nitrates combustion method[J]. International Journal of Hydrogen Energy, 2014, 39(25): 13141-13155.

1   [42]. Nikolla E, Holewinski A, Schwank J, et al. Controlling carbon surface chemistry

2   by alloying: carbon tolerant reforming catalyst[J]. Journal of the American

3   Chemical Society, 2006, 128(35): 11354-11355.

4   [43]. Twigg M V, Spencer M S. Deactivation of copper metal catalysts for methanol

5   decomposition, methanol steam reforming and methanol synthesis[J]. Topics in

6   Catalysis, 2003, 22(3): 191-203.

7   [44]. Koike M, Li D, Watanabe H, et al. Comparative study on steam reforming of

8   model aromatic compounds of biomass tar over Ni and Ni–Fe alloy

9   nanoparticles[J]. Applied Catalysis A: General, 2015, 506: 151-162.

10   [45]. Mardilovich P P, She Y, Ma Y H, et al. Defect-free palladium membranes on

11   porous stainless-steel support[J]. AIChe journal, 1998, 44(2): 310-322

12

1 **Table 1. Pore structure parameters of samples.**

Samples	BET Surface Area $(m^2 \cdot g^{-1})$	Pore volume $(cm^3 \cdot g^{-1})$	Pore width (nm)
Al_2O_3	274.31	0.3456	5.04
Al_2O_3-H	243.63	0.3512	6.92
Cu/Al_2O_3	224.21	0.3623	6.46
$CuCe/Al_2O_3$	219.33	0.3402	6.20
$CuCe/Al_2O_3$-H	254.36	0.3576	6.69
Porous ceramics support	0.93	0.0042	16.94
Supported palladium membranes	1.33	0.0058	16.72

2

3

1

Table 2. Elemental composition and content of each catalyst (wt.%).

Catalysts	Composition (wt.%)			
	O	Cu	Al	Ce
Cu/Al$_2$O$_3$	27.65	21.64	50.71	/
CuCe/Al$_2$O$_3$	8.95	35.72	11.24	44.09
CuCe/Al$_2$O$_3$-H	31.31	5.15	41.50	22.05

2

3
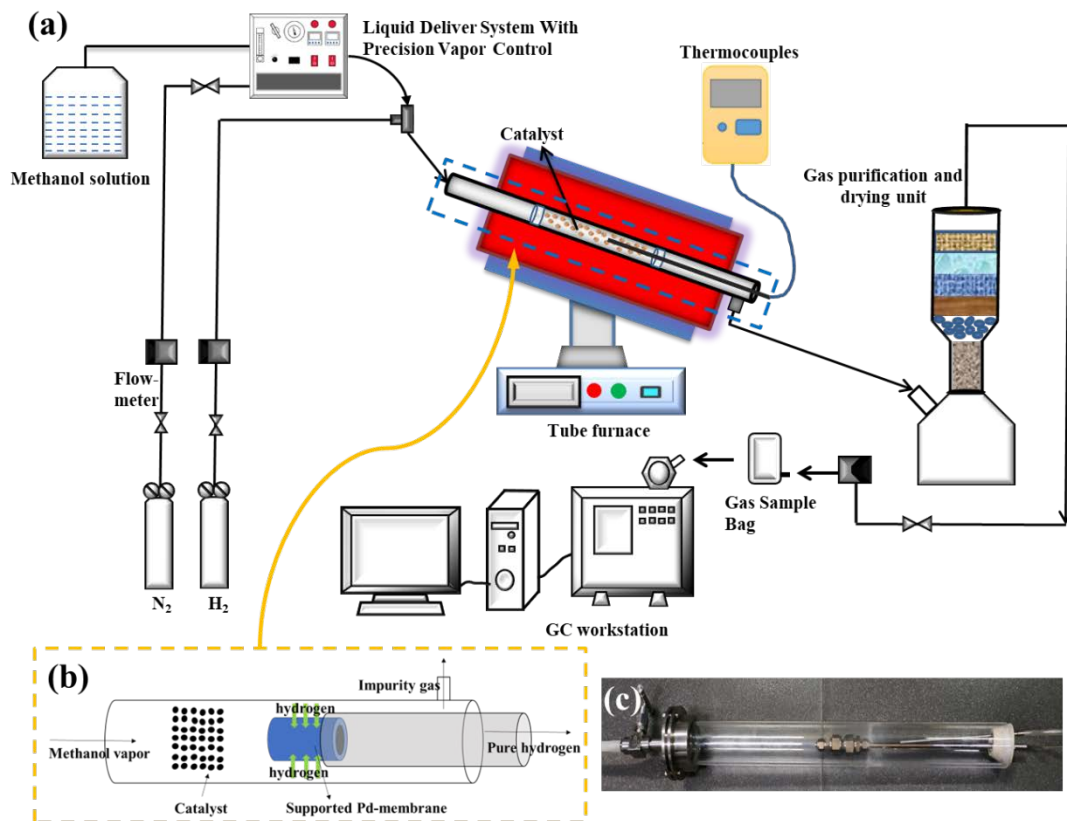
Fig. 1. (a) Schematic diagram of the test apparatus on a fixed-bed reactor for methanol steam reforming reaction; (b) Schematic diagram and (c) photograph of the hydrogen-purification integrated reactor.

1

2
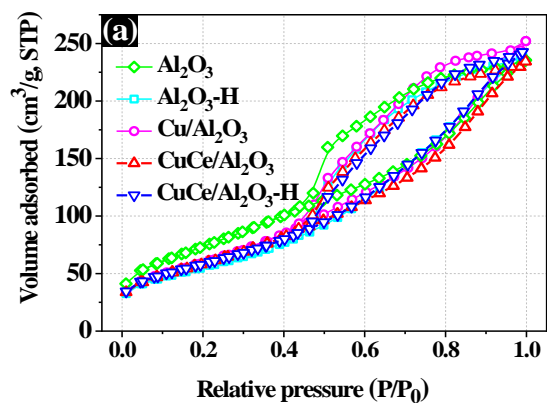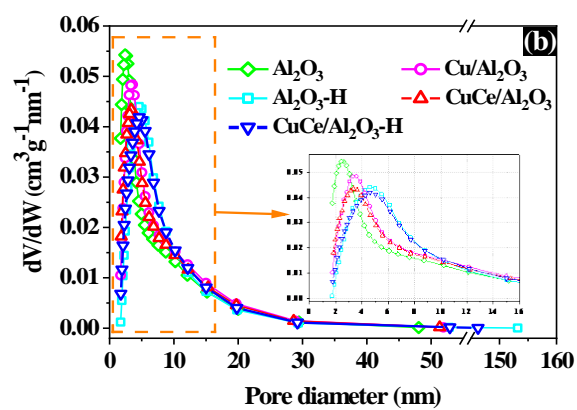
Fig. 2. (a) N$_2$ adsorption isotherm and (b) pore size distribution of synthetic

catalysts.

5

6
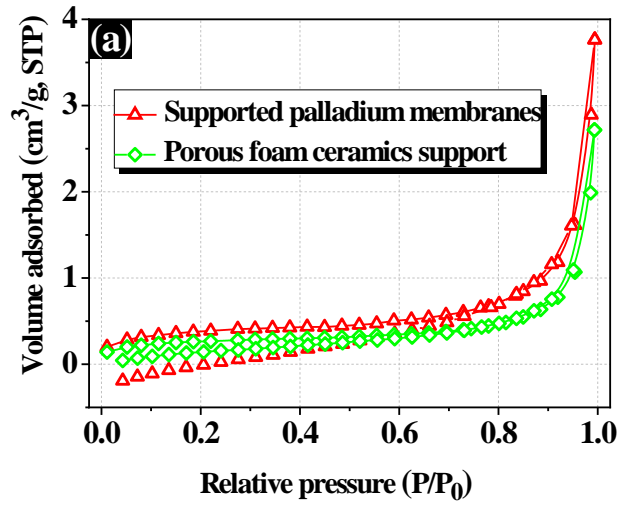
1
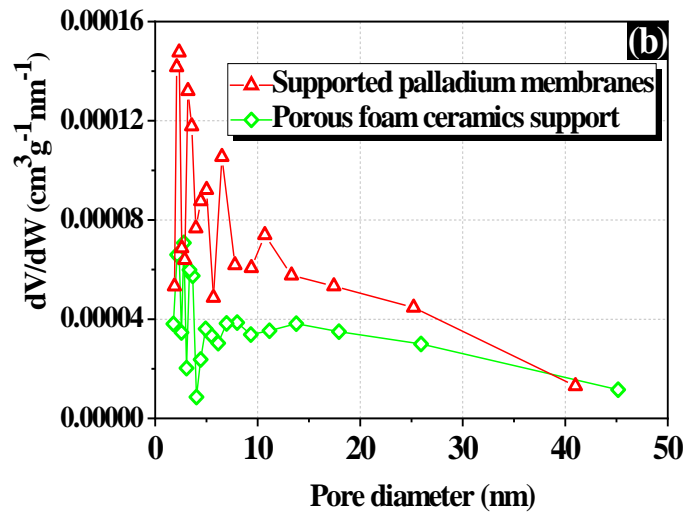
2

3 **Fig. 3. (a) N_2 adsorption isotherm and (b) pore size distribution of supported**

4 **palladium membranes.**

5

6
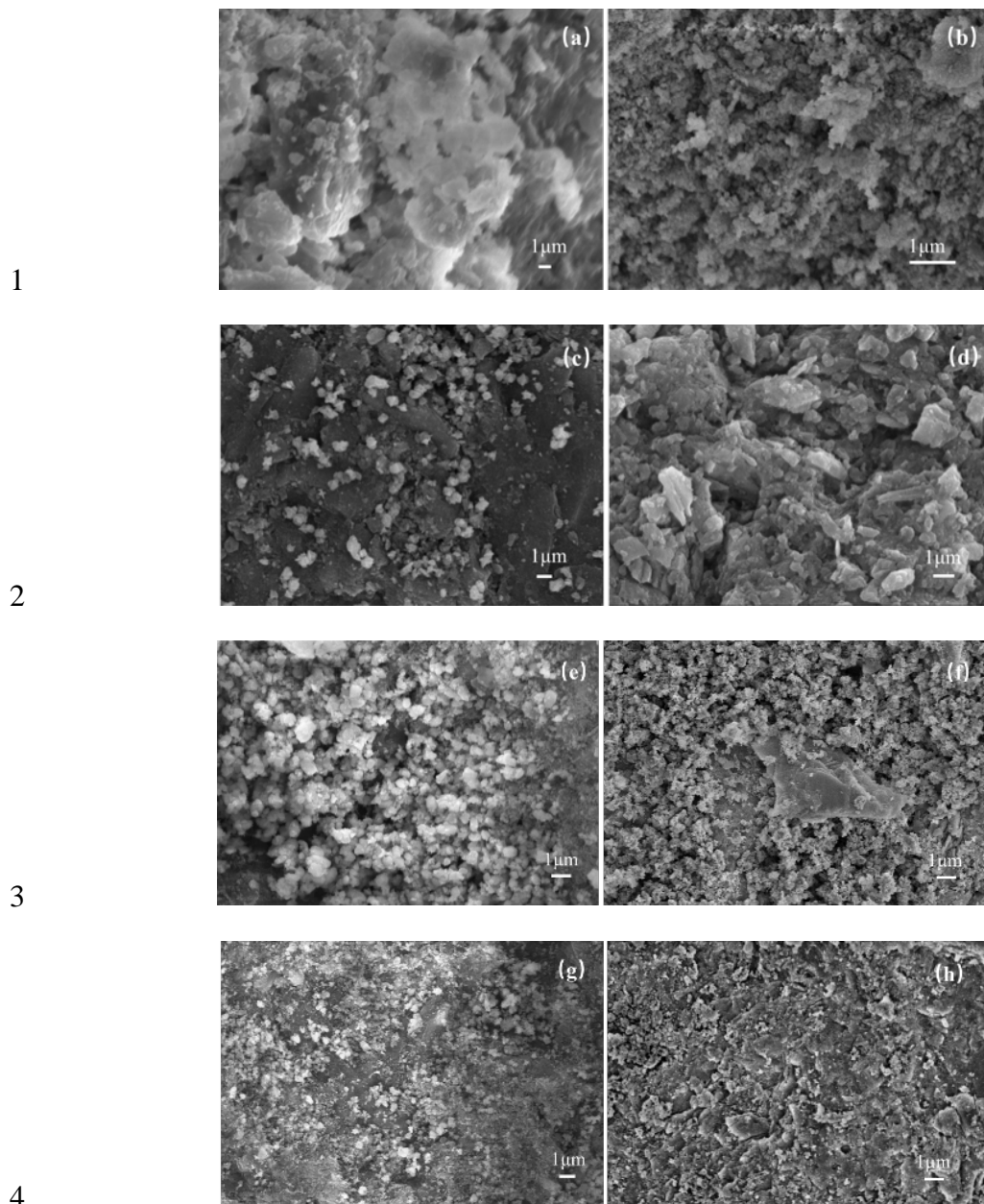
Fig. 4. SEM images of: (a) Al_2O_3; (b) Al_2O_3-H; (c) fresh Cu/Al_2O_3; (d) spent Cu/Al_2O_3; (e) fresh $CuCe/Al_2O_3$; (f) spent $CuCe/Al_2O_3$; (g) fresh $CuCe/Al_2O_3$-H; (h) spent $CuCe/Al_2O_3$-H.
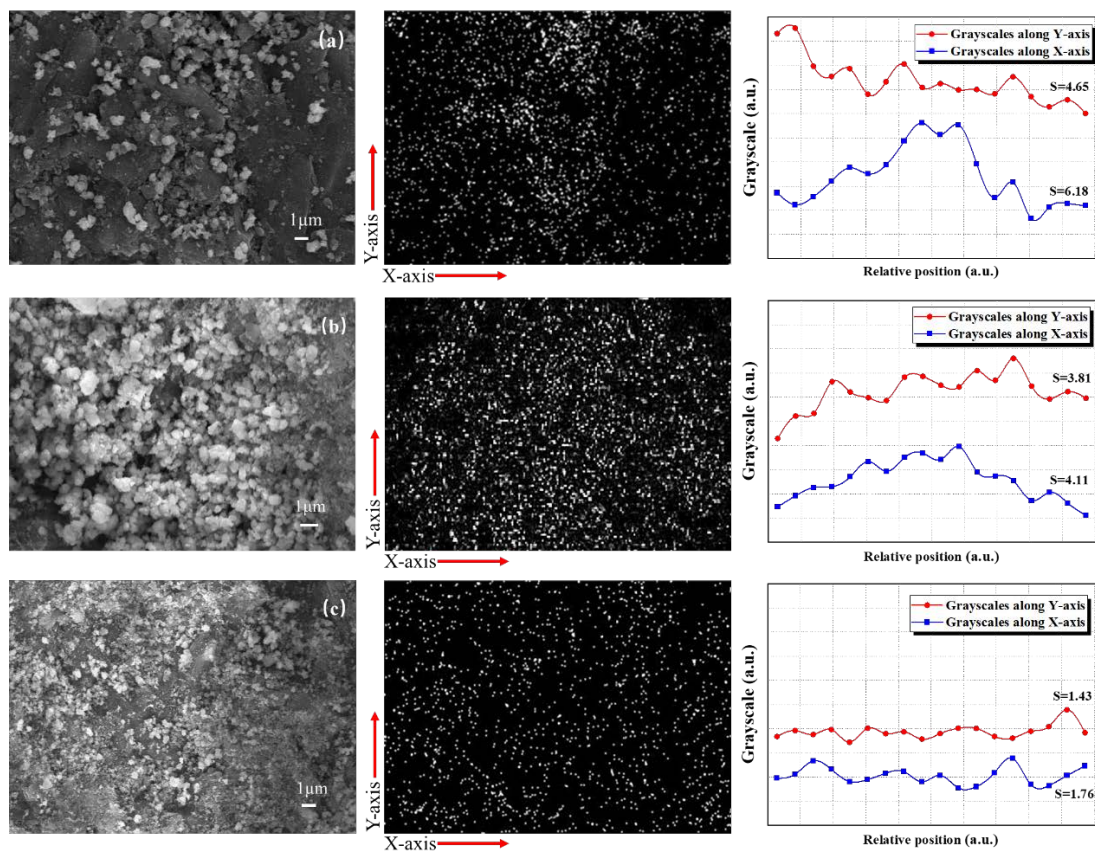
Fig. 5. Copper element mapping and grayscale distribution for fresh (a) Cu/Al$_2$O$_3$, (b) CuCe/Al$_2$O$_3$ and (c) CuCe/Al$_2$O$_3$-H.
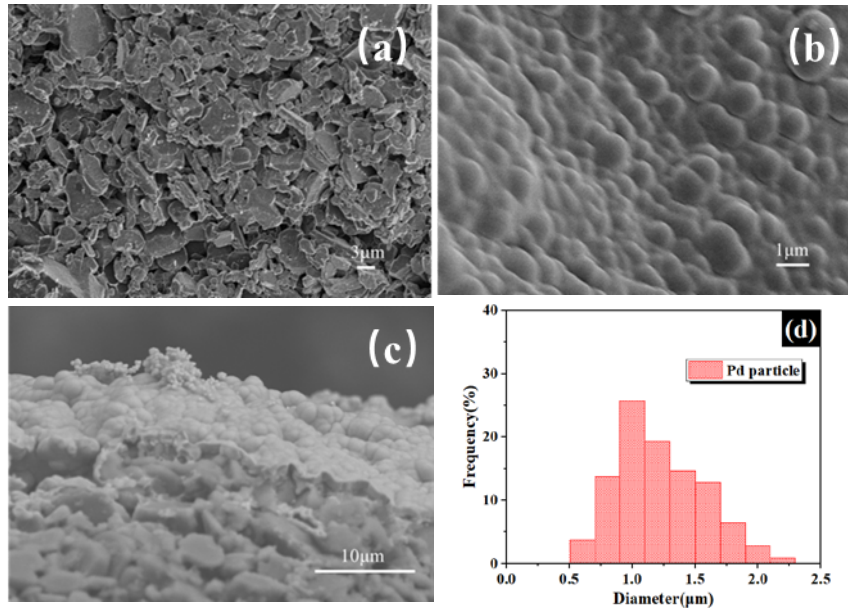
Fig. 6. SEM micrographs of (a) porous ceramics support and supported palladium membranes: (b) top surface (c) cross section; (d) Pd particle size distribution of top surface.
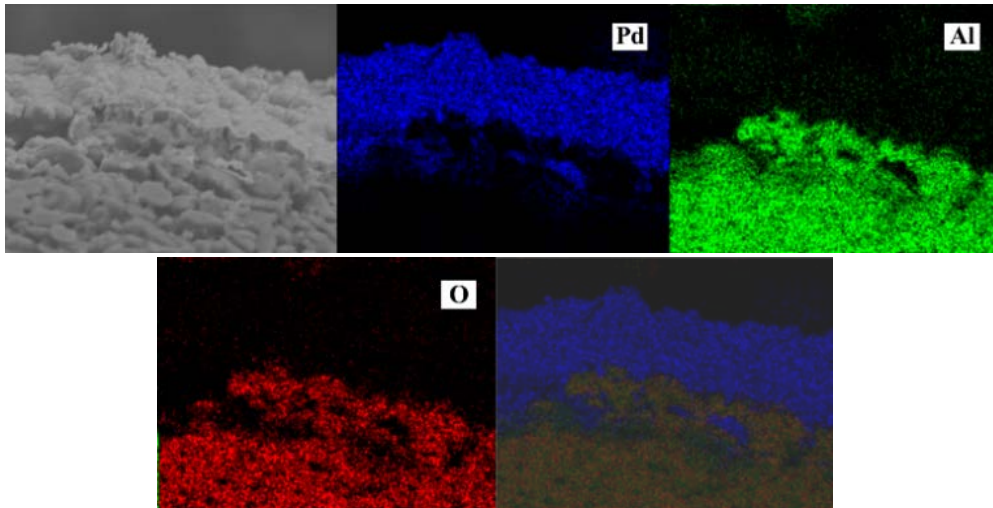
1

2   **Fig. 7. Element mapping for cross section of the supported palladium**

3   **membranes.**

4

5
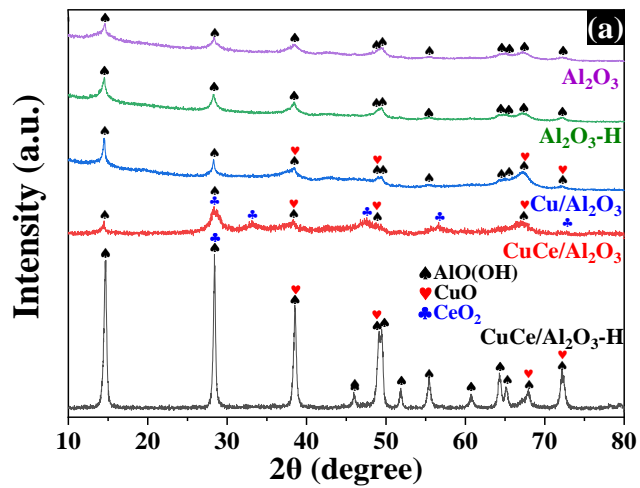
1
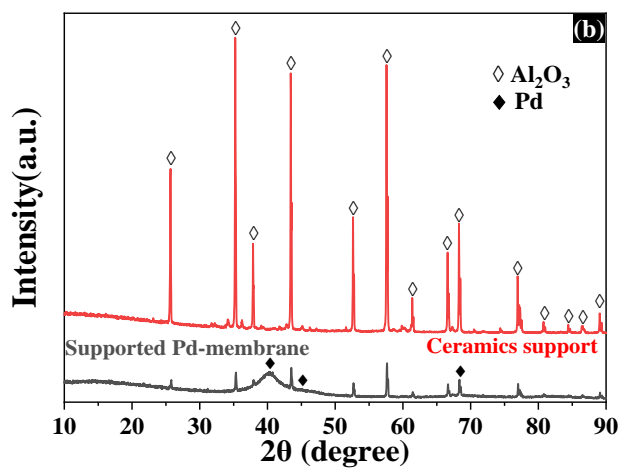
2

3   **Fig. 8. XRD pattern of (a) synthetic catalysts and (b) supported palladium**

4   **membranes.**

5

6
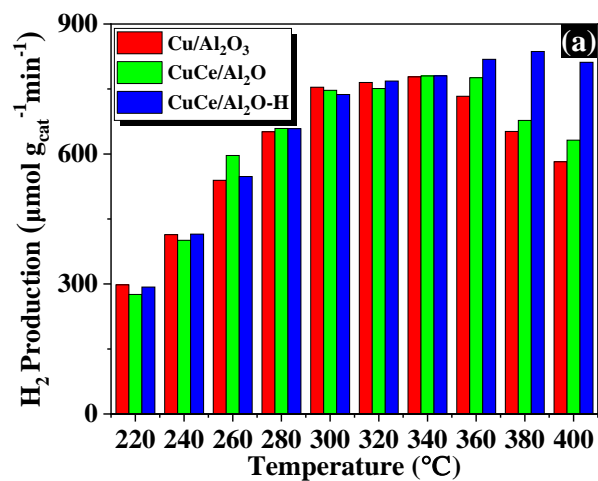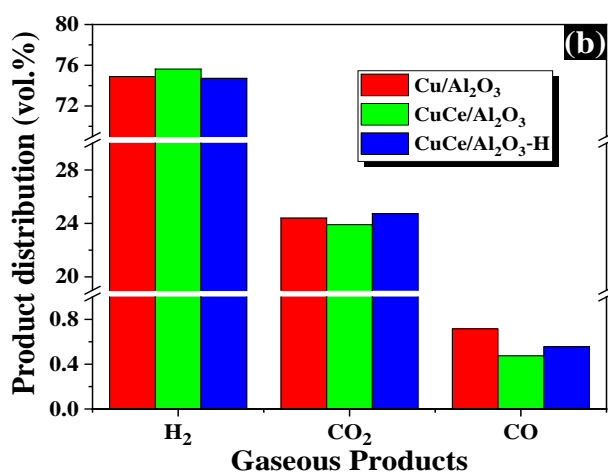
Fig. 9. (a) H₂ production of Cu/Al₂O₃, CuCe/Al₂O₃ and CuCe/Al₂O₃-H at different temperatures and (b) gaseous product distribution at 300 °C of catalysts.

1
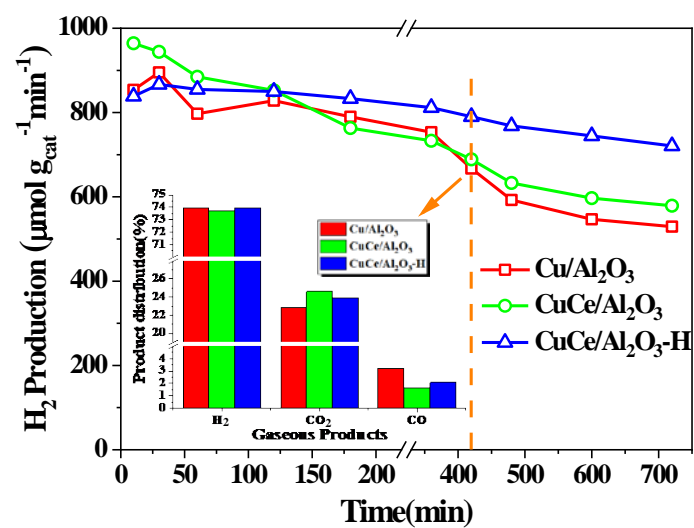
Fig. 10. Hydrogen production of catalysts under 400 °C for 720 min; the

gaseous product distribution at 420 min (insert).

4

5

1
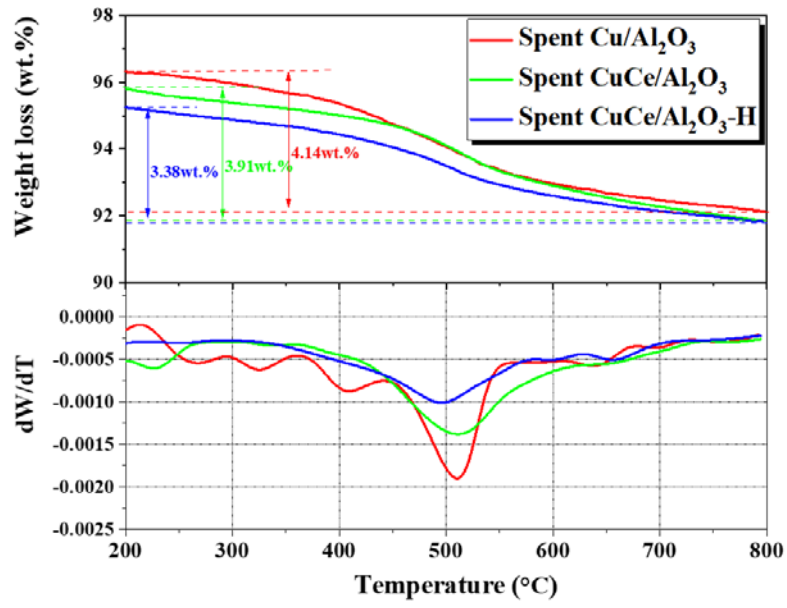
Fig. 11. TG-DTG curves of spent catalysts under the heating rate of
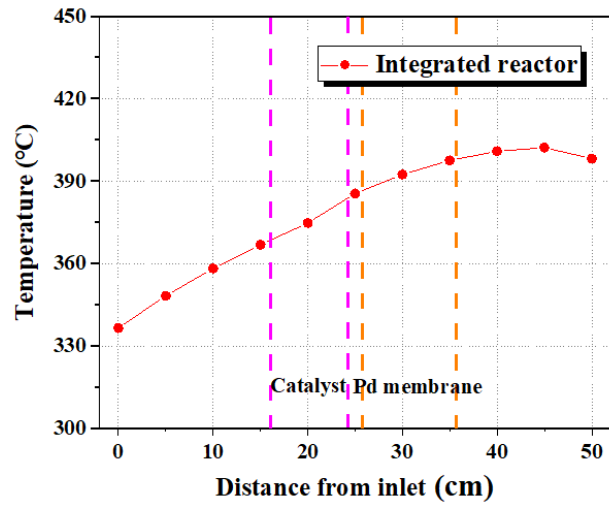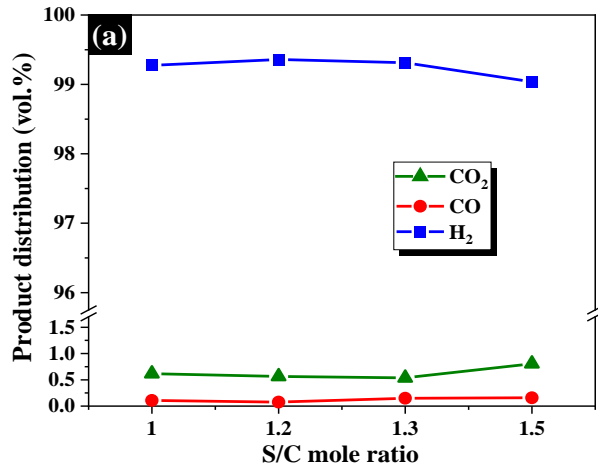
10 °C/min.

1

2
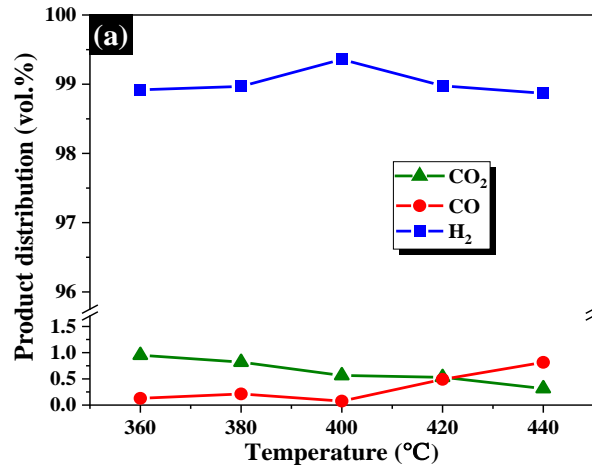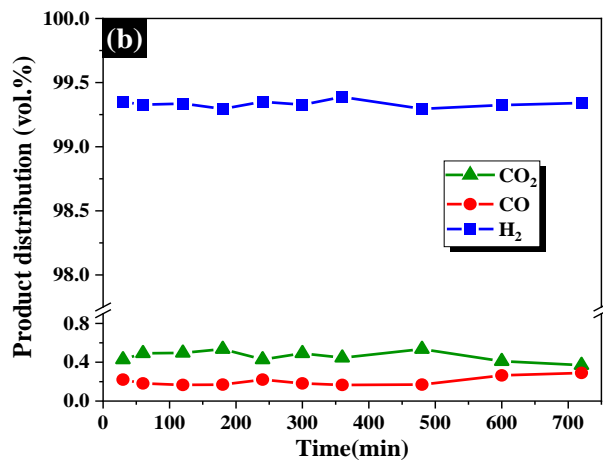
3   **Fig. 12. (a) Gaseous product distribution of the hydrogen-purification**

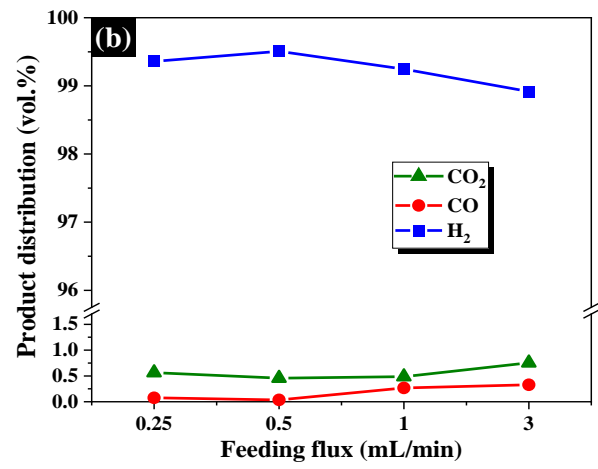4   **integrated reactor at different temperatures and (b) under 400 °C for 720 min.**

5

6

Fig. 13. Internal temperature distribution of the hydrogen-purification integrated reactor at 400 °C.

1

2

3   **Fig. 14. Gaseous product distribution of the hydrogen-purification**

4   **integrated reactor at (a) different S/C mole ratio and (b) different feeding flux.**

5